Biosensors and Bioelectronics 92 (2017) 661–667

Contents lists available at ScienceDirect

Biosensors and Bioelectronics

journal homepage: www.elsevier.com/locate/bios

Enzyme-polyelectrolyte multilayer assemblies on reduced graphene oxide field-effect transistors for biosensing applications

Esteban Piccinini[a,1], Christina Bliem[b,1], Ciril Reiner-Rozman[c], Fernando Battaglini[d], Omar Azzaroni[a,*], Wolfgang Knoll[c]

[a] Instituto de Investigaciones Fisicoquímicas Teóricas y Aplicadas (INIFTA) – Departamento de Química, Facultad de Ciencias Exactas, Universidad Nacional de La Plata – CONICET, Suc. 4, CC 16, La Plata, Argentina
[b] Centre of Electrochemical Surface Technology (CEST), Viktor-Kaplan-Straße 2, 2700 Wiener Neustadt, Austria
[c] AIT Austrian Institute of Technology, Donau City Straße 1, 1220 Vienna, Austria
[d] INQUIMAE, Departamento de Química Inorgánica, Analítica y Química Física, Facultad de Ciencias Exactas y Naturales, Universidad de Buenos Aires, Ciudad Universitaria, Buenos Aires, Argentina

ARTICLE INFO

Keywords:
Graphene
Field-effect transistors
Chemical sensors
Biosensors

ABSTRACT

We present the construction of layer-by-layer (LbL) assemblies of polyethylenimine and urease onto reduced-graphene-oxide based field-effect transistors (rGO FETs) for the detection of urea. This versatile biosensor platform simultaneously exploits the pH dependency of liquid-gated graphene-based transistors and the change in the local pH produced by the catalyzed hydrolysis of urea. The use of an interdigitated microchannel resulted in transistors displaying low noise, high pH sensitivity (20.3 μA/pH) and transconductance values up to 800 μS. The modification of rGO FETs with a weak polyelectrolyte improved the pH response because of its transducing properties by electrostatic gating effects. In the presence of urea, the urease-modified rGO FETs showed a shift in the Dirac point due to the change in the local pH close to the graphene surface. Markedly, these devices operated at very low voltages (less than 500 mV) and were able to monitor urea in the range of 1–1000 μm, with a limit of detection (LOD) down to 1 μm, fast response and good long-term stability. The urea-response of the transistors was enhanced by increasing the number of bilayers due to the increment of the enzyme surface coverage onto the channel. Moreover, quantification of the heavy metal Cu^{2+}(with a LOD down to 10 nM) was performed in aqueous solution by taking advantage of the urease specific inhibition.

1. Introduction

Graphene, a two-dimensional zero band gap semiconducting material, has gained vast interest in material science, energy storage and sensor technology, due to its remarkable electronic and mechanical properties (Choi and Lee, 2012). Its high carrier mobility and ambipolar field effect (Cai et al., 2014), together with a great sensitivity towards changes in environmental conditions makes graphene perfectly suitable as transducing material for the use in chemical sensors. Graphene based field effect transistors (FETs) have been applied for pH sensing (Ohno et al., 2009; Sohn et al., 2013), DNA (Dong et al., 2010) and protein detection (Reiner-Rozman et al., 2015), as well as for the enzymatic detection of small molecules like glucose (Zhang et al., 2015) or dopamine (He et al., 2010). In particular, biosensors based on solution-gated graphene transistors (SGGTs) have gained much attention in clinical diagnosis because they are suitable for real-time, high-throughput and highly sensitive detections (Yan et al., 2014).

Owing to its defective structure and the remaining functional groups, reduced graphene oxide (rGO) is extremely advantageous for pH sensing (Sohn et al., 2013; Reiner-Rozman et al., 2015). This pH dependency is caused by two factors: the interaction of functional groups at the rGO surface, such as –OH and –COOH groups, with H^+ ions of the electrolyte (Sohn et al., 2013) giving rise to a change in the surface charge density, and the change of the Gouy-Chapman diffuse electric double layer causing electrostatic gating effects (Reiner-Rozman et al., 2015). This intrinsic property of rGO can easily be exploited for biosensing purposes, but only few studies focused on this approach (Sohn et al., 2013; Hess et al., 2014).

As the biosensor performance strongly depends on the characteristics of the interfacial architecture, the biomolecules must be immobilized by means of a process that guarantees the maintenance of the biological activity and the accessibility to the active sites. To date, most

* Corresponding author.
E-mail addresses: azzaroni@inifta.unlp.edu.ar (O. Azzaroni).
[1] These authors contributed equally to this work and should be considered as co-first authors.

http://dx.doi.org/10.1016/j.bios.2016.10.035
Received 12 August 2016; Received in revised form 28 September 2016; Accepted 18 October 2016
Available online 21 October 2016

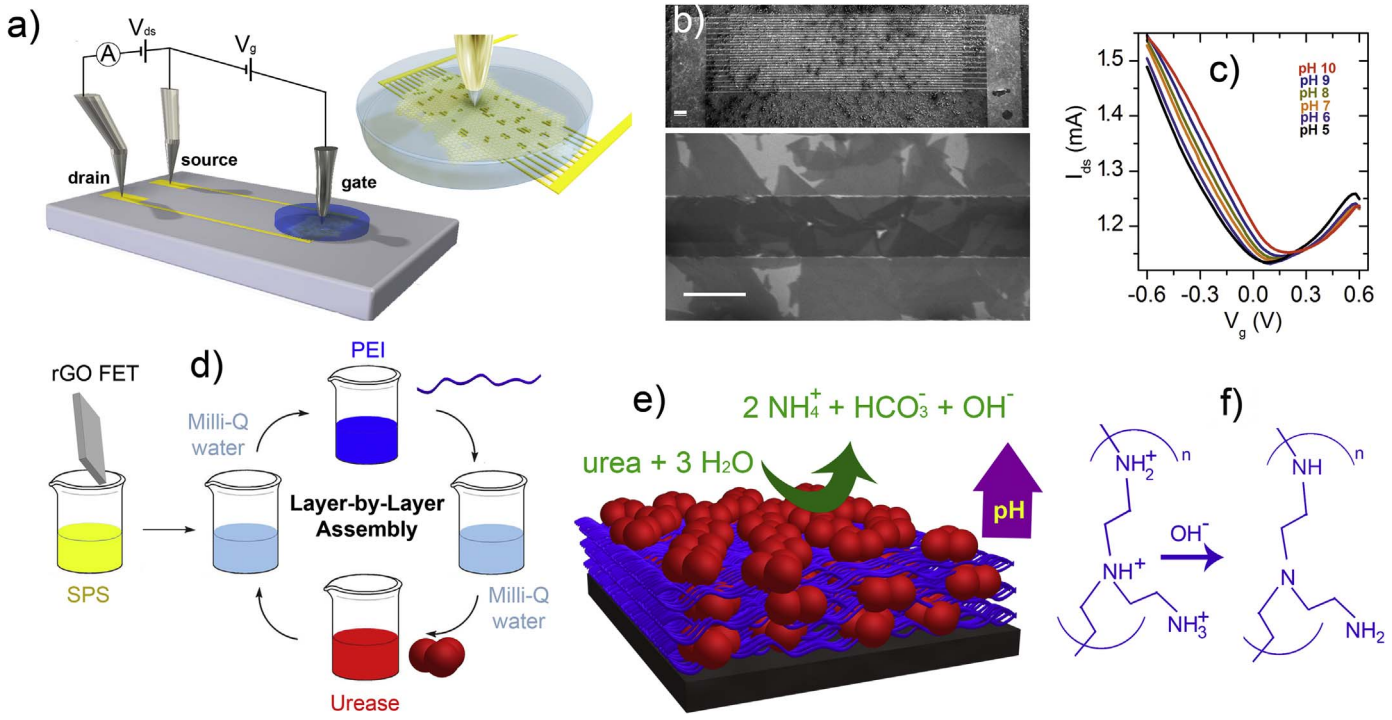

Fig. 1. (a) Illustration of the solution gated rGO FET and the interdigitated channel. (b) SEM images of an interdigitated channel modified with rGO: scale bar =100 μm (top) and scale bar =10 μm (bottom) (c) Transfer characteristics of a SPS-modified rGO FET obtained at a fixed V_{ds} (0.1 V) in 10 mM KCl and 0.1 mM HEPES solution with pH varying from 5 to 10. (d) Schematic of the LbL deposition process. (e) Schematic of the urease-PEI multilayer film and the urease-catalyzed hydrolysis of urea. (f) Change in the degree of protonation of PEI with increasing pH.

of the research efforts in graphene-based FETs biosensors focused on the immobilization of biomolecules by covalent binding to functional groups of graphene or to a linker molecule (Zhan et al., 2014). However, covalent attachment can disrupt the folding and functionality of the native biomolecule if essential groups are involved in the immobilization (Sheldon and Van Pelt, 2013; Scouten et al., 1995). Furthermore, the covalent attachment of molecules can induce damage to the sp^2 structure of graphene (Niyogi et al., 2010). In this regard, layer-by-layer (LbL) assembly offers a versatile and simple bottom-up technique for the fabrication of functional thin films on solid substrates through a wide variety of non-covalent interactions: electrostatic (Cortez et al., 2014; Decher and Hong, 1991), molecular recognition (Pallarola et al., 2010; Piccinini et al., 2015), and others (Ariga et al., 2007). Particularly, the LbL assembly through electrostatic interactions has been firmly established as a general method for alternately depositing dense layers of charged molecules onto oppositely charged surfaces (Decher and Schlenoff, 2012). The concept of the approach relies on the attractive forces between oppositely charged molecules. Furthermore, the incorporation of enzymes to the LbL assemblies led to enormous progress in the field of bioelectronics due to their inherent structural and functional properties (Rydzek et al., 2014). In fact, a large number of electrochemical enzyme-based biosensors using different techniques (e.g., potentiometry, voltammetry and others) were developed (Iost and Crespilho, 2012). Nevertheless, to the best of our knowledge, no LbL assemblies onto graphene field-effect transistors have been reported for the development of biosensors.

Urea concentration in biological solutions (blood and urine) is a relevant indicator of the functional condition of the human organism. Its value is indispensable for the diagnosis and control of a number of kidney and liver diseases (Carvounis et al., 2002; Lakard et al., 2011; Nguyen et al., 2016; Zhybak et al., 2016) and, therefore, the measurement of urea concentration is a routine procedure in clinical practice. Of particular interest are the cases of haemodialysis patients, since real-time urea monitoring may improve the diagnosis of kidney failure as well as prolong the patient's life expectancy (Sant et al., 2011). Although various urea assay systems have been designed based on different physicochemical principles (such as fluorescence, colorimetric, potentiometry methods (Rajesh et al., 2005; Singh et al., 2008), most of them require a sample pretreatment, the use of expensive equipments or laborious procedures and they cannot be used for on-line monitoring. In this sense, the use of SGGTs seems to be a more advantageous approach since this method include the following attractive features: real-time response, operation in aqueous solutions at very low voltages (less than 1 V, which is elemental for biological sensing), and higher sensitivity than conventional electrochemical methods because of their inherent amplification property (Zhang et al., 2015).

In this work we describe the construction of urease-polyethylenimine (PEI) multilayer assemblies onto the interdigitated microchannel of rGO FETs for the enzymatic detection and determination of urea. As this biosensor platform exploits the pH dependency of liquid-gated graphene-based transistors, the transfer characteristics of rGO FETs were studied as a function of pH. Moreover, we demonstrate that the PEI layer onto the channel acts as a transduction unit, thus, amplifying the pH response of the transistors. In the presence of urea, a significant voltage shift in the bipolar transfer characteristics of graphene can be measured due to the change in pH value resulting from the catalyzed hydrolysis of urea. These devices were able to monitor urea in the range of 1–1000 μm, with a limit of detection (LOD) down to 1 μm. The increment of the number of urease/PEI bilayers and its influence on the urea-response was also studied. Finally, quantification of the heavy metal Cu^{+2} was performed by taking advantage of the urease specific inhibition.

2. Materials and methods

The following chemicals and reagents were used in the experiments: urease from Canavalia ensiformis (Jack Bean) type IX (50,000–100,000 units/g, Sigma-Aldrich), branched polyethylenimine (M_n= 10,000, Aldrich), hydrazine monohydrate (99%, Sigma-Aldrich), (3-

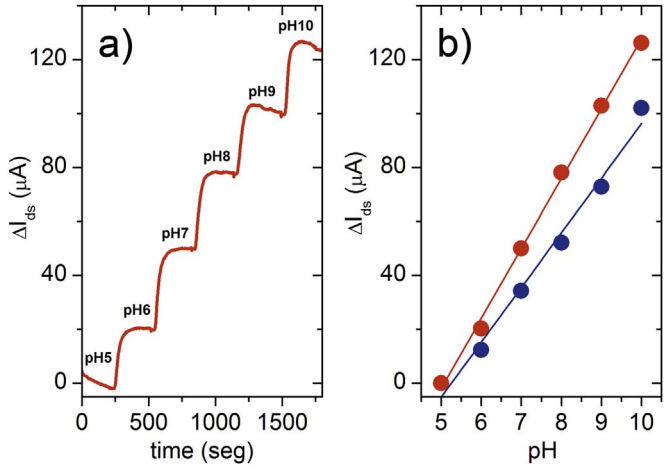

Fig. 2. (a) Change in the channel current (ΔI_{ds}) of a SPS/PEI-modified rGO FET monitored in real-time varying the pH from 5 to 10 (b) ΔI_{ds} as a function of pH for a SPS-modified rGO FET (blue circles) and a SPS/PEI-modified rGO FET (red circles). Experimental conditions: flow rate =300 μl/min, V_g=−0.2 V and V_{ds}=0.1 V. (For interpretation of the references to color in this figure legend, the reader is referred to the web version of this article.)

Aminopropyl)-triethoxysilane (97%, Sigma-Aldrich), urea (99%, Sigma), HEPES (Sigma), Copper (II) sulfate anhydrous (99%, Sigma), sodium 1-pyrenesulfonate (97%, Sigma). Interdigitated gold microelectrodes (ED-IDA1-Au) and an electrochemical flow-cell were purchased from Micrux Technologies. Solutions of 10 mM KCl and 0.1 mM HEPES were prepared at different pH (adjusted using KOH or HCl solutions). The high [KCL]/[HEPES] ratio ensured almost a constant ionic strength independent of pH. Urea solutions were prepared in 10 mM KCl and 0.1 mM HEPES at pH 6.

2.1. gFET fabrication

The glass area between the interdigitated microelectrodes (10 μm×55.2 mm) was functionalized with rGO and it served as the channel in the field effect transistor (Fig. 1a). First, the glass area was functionalized with a self-assembled monolayer of (3-Aminopropyl) triethoxysilane (APTES). For this purpose, the microelectrodes were incubated in an ethanolic solution of 2% APTES for 1 h, rinsed with ethanol and annealed for 2 h at 120 °C. Graphene oxide flakes prepared by a modified Hummer's method (Reiner-Rozman et al., 2015) were used. An aqueous dispersion of graphene oxide (GO) flakes was drop-cast on top of the functionalized microelectrodes and incubated for 2 h. Reduction of the GO was accomplished by using hydrazine at 80 °C overnight (Reiner-Rozman et al., 2015). Fig. S1 shows the deconvoluted C1s spectra before (left) and after (right) the GO reduction obtained by X-ray spectroscopy. A significant increase of the C–C/C=C (284.6 eV) relative intensity was observed after reduction.

2.2. Layer-by-layer assembly

In order to confer negative charge to the graphene surface, the rGO FETs were incubated overnight in 5 mM sodium 1-pyrenesulfonate (SPS) in dimethylformamide (DMF), then rinsed three times with DMF and deionized water. Layer-by-layer (LbL) assemblies mediated by electrostatic interactions were built up onto the SPS-modified rGO FETs by alternate adsorption of polyethylenimine (a polycation) and urease (negatively charged at physiological pH) as reported by others (Forrest et al., 2005). First, the SPS-modified rGO FETs were incubated in an aqueous solution of 2 mg/ml polyethylenimine (PEI) at pH 8.5 for 10 min, and rinsed with deionized water. Then, the gFETs were incubated in 1 mg/ml urease in buffer (0.1 mM HEPES and 10 mM KCl adjunted at pH 7.4) for 30 min, followed by rinsing with deionized water. More than one bilayer was prepared by repeating the PEI and urease adsorption as a cycle.

2.3. Measurement set-up

Interdigitated gold microelectrodes (Fig. 1b) were used as source and drain electrodes, and a silver wire was used as gate. Liquid-gated graphene FETs were measured using an electrochemical flow-cell (Micrux instruments) for automatic sample collection and a peristaltic pump (Ismatec) to assure a constant flow rate of 300 μl min^{-1}. Electrical measurements were performed by means of a probe station (Keithley 4200) applying 100 mV source-drain bias (V_{sd}). Scanning electron microscopy (SEM) images were recorded in order to monitor the rGO distribution and the reduction of the GO using a SUPRA 40 Field Emission Scanning Electron Microscope (Zeiss).

2.4. Charge carrier mobility of the rGO FETs

The charge carrier mobility (μ) of the devices was calculated from this equation (Wang and Burke, 2013):

$$\mu = (L/WC_g V_{ds})(\Delta I_{ds}/\Delta V_g) \quad (1)$$

where L and W are the channel length =10 μm and the channel width =55.2 mm, C_g is the top-gate capacitance and $\Delta I_{ds}/\Delta V_g$ is the rate of change of I_{ds} with respect to V_g (transconductance). The C_g value (57 nF cm^{-2}) can be obtained considering it as a series of the quantum capacitance of graphene (C_Q) and the electrostatic gate capacitance (C_{GT}) (Ohno et al., 2009).

3. Results and discussion

Liquid-gated rGO FETs (Fig. 1a) were fabricated by using interdigitated gold microelectrodes (Fig. 1b top) with 10 μm channels and a total channel width of 52.2 mm. In this configuration, the narrow channel geometry assures the source-drain contact by assembled rGO flakes (Fig. 1b bottom), resulting in devices with low noice and high transconductance (up to 800 μS) (Fig. 2S). It is important to highlight that the transconductance of our devices is significantly higher than reported for other rGO FETs (Sohn et al., 2013; He et al., 2010; Reiner-Rozman et al., 2015; Kim et al., 2013). It was reported that a high transconductance is a fundamental feature for the development of transistors with enhanced sensitivity for sensing applications (Zhang et al., 2015). Moreover, the special channel arrangement assures a very good device to device reproducibility, which is crucial for realistic applications.

A plot of drain-source current (I_{ds}) as a function of the gate-source voltage applied (V_g) and under a fixed source-drain potential (V_{ds}) for a rGO FET is shown in the Fig. 1c. The application of an external electric potential (e.g., the gate potential) can shift the Fermi energy of the rGO (Wong and Akinwande, 2011), and therefore modulate the charge carriers density, which results in a change of I_{ds}. The minimum I_{ds} (Dirac point, V_i) at pH 6 (purple curve in Fig. 1c) is found at V_g=95 mV. At V_i, the majority of the charge carriers change from holes ($V_g < V_i$) to electrons ($V_g > V_i$). The charge carrier mobility (μ) of the device was calculated as explained by others (Wang and Burke, 2013), obtaining values of 30 $cm^2 V^{-1} s^{-1}$ for holes and 15 $cm^2 V^{-1} s^{-1}$ for electrons. These values are in concordance with other rGO FETs (Sohn et al., 2013; Gómez-Navarro et al., 2007).

The integration of enzymes on the surface of a sensor is an attractive approach for the detection of specific substrates. Nevertheless, covalent attachment of biomolecules onto graphene can induce damage to the sp^2 structure of graphene (Niyogi et al., 2010) and disrupt the folding and functionality of the native biomolecule if essential groups are involved in the immobilization (Sheldon and Van Pelt, 2013; Scouten et al., 1995). For this reason, the electrostatic layer-by-layer assembly approach was used for the non-covalent immobiliza-

tion of the enzyme urease onto the channel of the rGO FETs. The whole preparation process of the urease-PEI multilayer assembly (referred to as $(PEI/urease)_n$) is schematized in the Fig. 1d. Since a charged surface is required for the initiation of the LbL assembly; the bare rGO-FETs were modified with a negative charged pyrene-based layer of sodium 1-pyrenesulfonate (SPS). The pyrene groups of the SPS attach to the graphene through π-π interactions, and on the other end the sulfonate groups retain a negative charge in a wide range of pH (at pH > 2) (Parviz et al., 2012).

As this type of enzyme sensor relies on the detection of small changes in pH during the enzymatic reaction, we studied the transfer characteristics of the transistors in a liquid-gated configuration under different pH values. Fig. 1c shows the transfer characteristics of a SPS-modified rGO FET in solutions with constant ionic strength and pH ranging from 5 to 10. Whereas the slope remained almost unchanged for both sides of the V_i, revealing that the charge mobility is nearly independent of the pH, a significant shift of V_i to more positive V_g values with increasing pH was observed. The V_i and the change in the I_{ds} (ΔI_{ds}) exhibited a linear dependence on pH with a slope of 23 ± 1.8 mV/pH (Fig. S3) and 20.3 ± 0.6 μA/pH (blue line Fig. 2b), respectively. Interestingly, the sensitivity (20.3 μA/pH) of our devices is almost one order of magnitude higher than for other reported graphene based FETs (Sohn et al., 2013; Reiner-Rozman et al., 2015; Ohno et al., 2009). As the sensitivity depends on the transconductance ($\Delta I_{ds}/\Delta V_g$), the high sensitivity value is mainly attributed to the use of interdigitated microchannels with short channel length (L) and large channel width (W) (see Eq. (1)). The transistors also showed remarkable electrical stability in pH sensing (Fig. S4), an important feature for the development of reliable sensors.

We proceeded with the assembly of a weak polycation onto the channel through electrostatic interactions. The SPS-modified transistors (referred to as rGO/SPS FETs) were incubated in an aqueous solution of polyethyleneimine, followed by rinsing with deionized water. After the PEI modification, the V_i shifted to a more negative gate voltage (blue line Fig. S5), i.e., −48 mV at pH 6. The change of the transfer characteristics after each step of polyelectrolyte LbL assembly was studied in detail by Wang and Burke (2014). The authors demonstrated that the deposition of a positive (or negative) polyelectrolyte layer on the gFET results in a negative (or positive) shift in the V_i. This behavior was attributed to the electrostatic gating effect of the charged polyelectrolyte layer. A PEI charge density of 0.011 C/m^2 was obtained for the first layer (details in ESI), consistent with reported literature values for polyelectrolyte multilayers (Wang and Burke, 2014).

Then, the effect of the PEI layer on the pH-response was studied. The transfer characteristics of a rGO/SPS/PEI field-effect transistor under different pH values were obtained (Fig. S6). Moreover, the real-time pH-response was monitored by I_{ds} as a function of time with biased V_g =−0.2 V and V_{ds} =0.1 V. Fig. 2a shows the titration curve in laminar flow (300 μl/min) increasing the pH of the solution after every 5 min. The I_{ds} increased by 126 μA for a change of pH from 5 to 10 (red line in Fig. 2b). Furthermore, a linear relationship (R =0.999) between the change in the I_{ds} (ΔI_{ds}) and the pH was found, exhibiting a sensitivity of 25.9 ± 0.6 μA/pH. Fig. 2b shows ΔI_{ds} as a function of the pH before and after the PEI assembly. Interestingly, the transistors modified with PEI showed an increase of the pH-response of almost 28%, from 20.3 μA/pH (before modification) to 25.9 μA/pH (after modification). Since PEI is a weak polycation (pK_a 8–9) (Von Harpe et al., 2000), the degree of protonation of the polymer decreases with increasing pH. If the degree of protonation of PEI is reduced, the charge density changes which results in p-doping by the electrostatic gating effect. A similar behavior was reported by Hess et al. (2014) for brushes of N,N-dimethylaminoethyl methacrylate groups on graphene-based FETs. Therefore, the weak polycation plays a double role: to act as a building block for the LbL assembly, and as a transducer element to amplify the detection of changes in the local pH.

Addition of organic molecules in solution can result in their adsorption to the graphene surface, leading to variations in the conductivity or in the charge carrier mobilities (He et al., 2010). Because of this, the non-specific response of the transistors to urea was examined prior to urease immobilization onto the PEI layer. Real-time measurements in the presence and absence of 10 mM urea were performed (Fig. S7). Without immobilized urease on the transistor, no distinguishable changes on I_{ds} were observed in the presence of urea.

After characterizing the FETs with respect to the pH-response, we proceeded with the enzyme urease immobilization by the LbL assembly approach. The rGO/SPS/PEI transistors were incubated in an aqueous solution of urease, followed by rinsing with deionized water. As reported by others, urease can be properly entrapped in PEI/urease multilayer assemblies with an efficient preservation of the enzyme activity, even for similar microchannels (Forrest et al., 2005). The urease modification onto the rGO/SPS/PEI FETs showed no alteration of the pH sensitivity and a negative V_i shift (red line Fig. S5), that is, an n-doping effect. Since the urease is negatively charged at pH > 5.2 (Krajewska, 2009), the observed direction of the shift is opposite to those expected for an electrostatic gating effect. Similar n-doping effects in graphene FETs were reported regarding the attachment of other negative biomacromolecules (Cai et al., 2014; Dong et al., 2010; He et al., 2010; Kim et al., 2013). Two mechanisms were suggested to explain this behavior: electron transfer from electron-rich molecules (Dong et al., 2010) or charged impurity scattering induced from charged molecules (Kim et al., 2013).

Further, the response of the transistors to the enzyme substrate (i.e., urea) was studied for a $(PEI/urease)_1$ assembly. Fig. 3a (top) shows the transfer characteristics in the absence (solid line) and in the presence (dashed line) of 100 μm urea. A clear shift of the V_i to more positive values was observed in the presence of urea, similar to the shift obtained upon increasing the pH of the solution. This result indicates that the enzyme properly catalyzed the hydrolysis of urea, which produces NH_4^+, HCO_2^- and OH^- (Fig. 1e) (Krajewska, 2009). As the hydroxyl ions, released during the enzyme activity, are involved in an acid-base equilibrium, a change of pH close to the urease is induced. This change of the local pH near the rGO, coupled to the variation of the charge density of the PEI, results in a significant shift of the V_i to more positive gate voltage.

The urea-response of the transistors was also examined in real-time (Fig. 3a bottom). A 100 μm urea solution was eluted for 4 min, allowing the I_{ds} to reach a plateau (referred as flow response), followed by stopping the flow (blue dashed line) during 1 min, where an I_{ds} peak can be observed (referred as static response). Then, the flow was resumed (green dashed line) which led to a drop in the I_{ds} current until the system returned to the flow steady-state condition. The I_{ds} response may be explained by mass transport phenomena as follows: in the flow condition, the hydroxyl ions obtained by the hydrolysis of urea are rapidly washed from the graphene surface mainly because of the forced convection (i.e., flux). A plateau in the I_{ds} is obtained when the ingress of urea to the film and egress of hydroxyl ions from the film reach a steady-state. When the flow is stopped, the egress of hydroxyl ions from the film is only governed by diffusion. This new condition yields an increment of the local hydroxyl ion concentration near the graphene surface until the urea concentration gradient reaches a maximum value, resulting in an I_{ds} peak. Fig. 3b shows the I_{ds} vs time response for gradually increasing concentrations of urea at a fixed gate bias (V_g =−0.2 V). In both conditions (flow and static) the increase of the I_{ds} with an increment of urea up to a concentration of 1 mM was observed. Above this concentration, the enzyme could be inhibited by the high substrate concentration and/or the alkaline local pH (Krajewska, 2009).

The nanoconstruction of enzyme-containing multilayered films turns out to be particularly attractive owing to the precise control over the loading of the enzyme. In order to increment the catalytic activity of

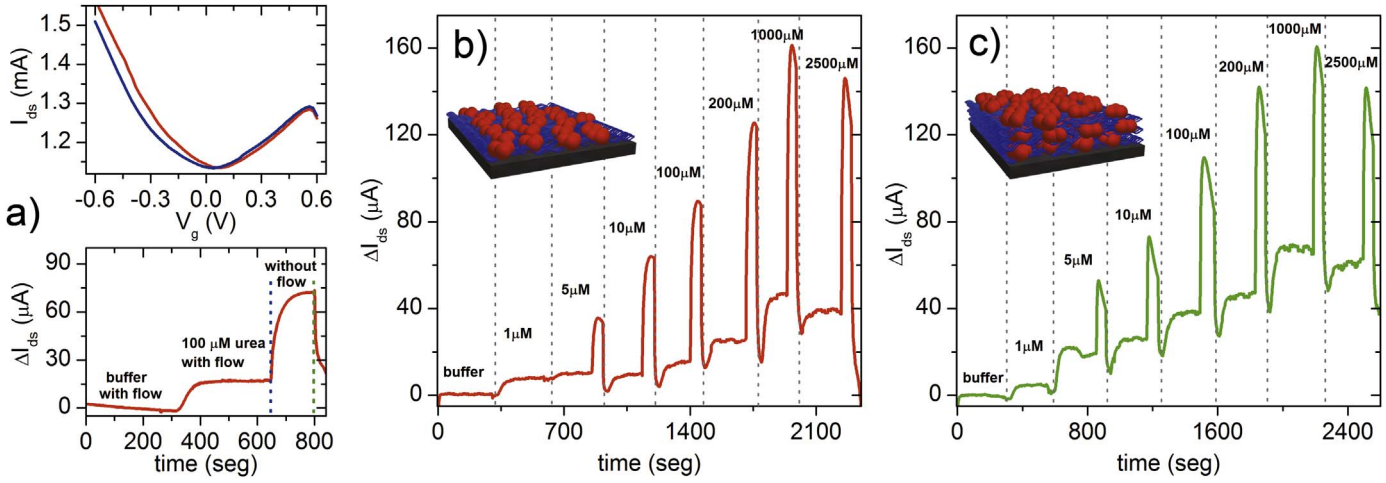

Fig. 3. (a) Transfer characteristics of a $(PEI/Urease)_1$ assembly in the absence (blue line) and in the presence (red line) of 100 μm urea (top), and the change in the channel current with and without flow (bottom). Channel current response (ΔI_{ds}) monitored in real-time for $(PEI/Urease)_1$ (b) and $(PEI/Urease)_3$ (c) LbL assemblies onto rGO FETs at different concentrations of urea. The marked line indicates the elution of the next concentration of urea. Experimental conditions: 10 mM KCl and 0.1 mM HEPES at pH 6, V_g =−0.2 V and V_{ds} =0.1 V. (For interpretation of the references to color in this figure legend, the reader is referred to the web version of this article.)

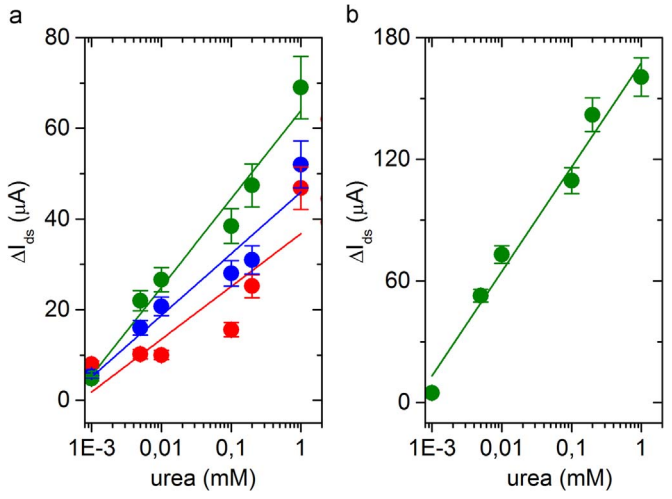

Fig. 4. (a) ΔI_{ds} of the flow response (flow rate =300 μl/min) as a function of the urea concentration for $(PEI/Urease)_1$ (red), $(PEI/Urease)_2$ (blue) and $(PEI/Urease)_3$ (green) LbL assemblies. (b) ΔI_{ds} of the static response as a function of the urea concentration for a $(PEI/Urease)_3$ LbL assembly. Experimental conditions: 10 mM KCl and 0.1 mM HEPES at pH 6, V_g =−0.2 V and V_{ds} =0.1 V. Error bars represent the standard deviation from measurements performed using three different devices. (For interpretation of the references to color in this figure legend, the reader is referred to the web version of this article.)

the film, $(PEI/urease)_n$ assemblies with two and three bilayers were constructed. A substantial improvement of the urea response was found for the $(PEI/urease)_2$ (Fig. S8) and the $(PEI/urease)_3$ (Fig. 3c) assemblies. The ΔI_{ds} signal as a function of the logarithmic urea concentration was determined from the flow response (Fig. 4a) as well as from the static response (Fig. 4b and Fig. S8). Although the flow response showed an ordinary linear relationship, a significant enhancement was achieved with the static response (e.g., R =0.987 for $(PEI/urease)_3$), with a limit of detection (LOD) below 1 μm. In flow condition, the sensitivity increased by 20% for two bilayers and by 68% for three bilayers, in comparison with one PEI/urease bilayer (see Fig. 4a). The latter suggests that the enzyme surface coverage increased with the number of bilayers, and therefore, higher changes in the local pH can be obtained in the presence of urea. For instance, $(PEI/urease)_3$ transistors showed a ΔI_{ds} of almost 70 μA (flow response) at 1 mM urea, indicating a change in the local pH from 6 to 8.7 (using the value of the pH sensitivity), consistent with other studies of urease entrapped in polymeric matrices (Tsai and Doong, 2005; Kazakova et al., 2011).

Table 1 shows a comparison of key analytical characteristics between our biosensor and other previously reported FET based urea biosensors. The FETs reported in this work showed outstanding properties, such as high sensitivity, wide operational range, low LOD and small applied potentials (V_g and V_{ds}). The performance of the $(PEI/urease)_3$-rGO FETs, including repeatability, reproducibility and stability, were also investigated. Relative standard deviation (RSD) for repeatability was 1.9% for six successive measurements of 100 μm urea. To study the sensor reproducibility, three $(PEI/urease)_3$-rGO FETs were prepared and the urea response was monitored in the range of 1–1000 μm. The sensor sensitivities exhibited a RSD of 5.8%, indicating good device-to-device reproducibility. It should also be pointed out that the developed biosensors showed a fast response and a good long-term stability, retaining almost 96% of the original response after 6 days of storage in buffer HEPES solution at 4 °C. The

Table 1
Analytical characteristics of different urease-FET based urea biosensors.

	Signal registration mode	LOD (μM)	Operational detection range (mM)	Sensitivity	Measurement configuration
Pan et al. (2009)	Nd_2TiO_5 based ion-sensitive FET	–	3–40	9.52 mV/mM	–
Sant et al. (2011)	pH/ChemFET	–	0.5–30	30 mV per decade of [urea]	V_{ds}=1 V, I_{ds}=0.1 mA
Yang et al. (2013)	Indium tin oxide based FET	500	1.5–10	62.4 mV per decade of [urea]	V_{ds}=0.5 V
Ahmad et al. (2015)	ZnO nanorods based FET	0.032	0.01–30	14.23 μA/cm^{2}mM	V_{ds}=0.1 V, V_g=4.5–6.0 V
Marchenko et al. (2015)	pH-sensitive FET	100	0.5–40	–	–
Melzer et al. (2016)	Carbon nanotubes based FET	50	0.01–10	–	V_{ds}=−0.4 V,V_g=−0.6 V
This work	Graphene based FET	1	0.001–1	9200 ± 500 μA/cm^2 per decade of [urea]	V_{ds}=0.1 V,V_g=−0.2 V

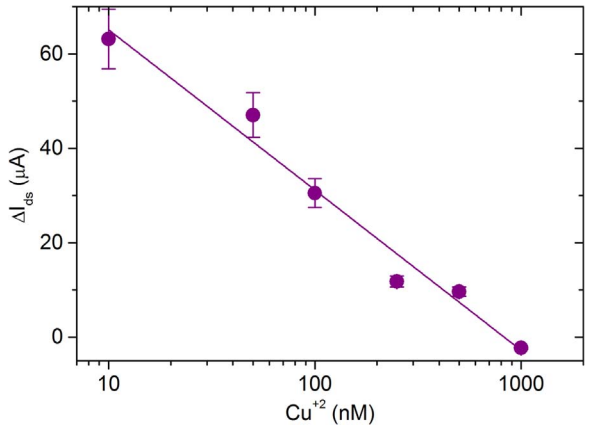

Fig. 5. ΔI_{ds} as a function of the Cu^{+2} concentration for a $(PEI/Urease)_3$ LbL assembly. The Cu^{+2} solutions contained 0.2 mM urea. Experimental conditions: 10 mM KCl and 0.1 mM HEPES at pH 6, flow rate =300 μl/min, V_g =−0.2 V and V_{ds} =0.1 V. Error bars represent the standard deviation from measurements performed using three different devices.

features of these devices may be of particular interest in view of an on-line urea monitoring for patients who are in a haemodialysis program (Sant et al., 2011).

The selectivity of a $(PEI/urease)_2$-rGO FET was evaluated in real-time by the elution of different blood interferences: dopamine, glucose, ascorbic acid and creatinine (Fig. S14). The elution of solutions containing interferences at concentrations near to those in blood samples led to negligible I_{ds} changes in comparison with the urea response. For example, 100 μm creatinine response corresponded to 3% of 100 μm urea response. Before the end of the elution step of each analyte, the flow was stopped for a few seconds. During this time period, the FET did not show significant I_{ds} changes in the presence of the interferences. Nevertheless, a significant increase of I_{ds} was obtained in the presence of urea. These facts evidence the good selectivity of the developed sensors in blood samples.

Finally, taking advantage of the inhibition of the urease activity, the transistors modified with $(PEI/urease)_3$ assemblies were evaluated for the quantification of heavy metals (details in the ESI). Fig. 5 shows the ΔI_{ds} as a function of the Cu^{+2} concentration in the presence of 0.2 mM urea. The increasing Cu^{+2} concentration led to a clear reduction of the ΔI_{ds}, and no enzymatic activity was exhibited above 1000 nM. As reported before, the Cu^{+2} ions strongly bind to cysteine and histidine residues which are critical for the urease activity, thus yielding the inhibition of the enzyme (Krajewska, 2008). A linear relationship between ΔI_{ds} and the logarithm of the Cu^{+2} concentration (R =0.985) with a LOD below 10 nM was found. The transistors showed a faster response, as well as a lower LOD (more than one order of magnitude), than previously reported heavy metal sensors based on urease (Tsai and Doong, 2005).

4. Conclusions

In this work we introduced the LbL assembly approach for the construction of polyelectrolyte-enzyme multilayer assemblies onto rGO FETs for biosensing applications. The graphene-based transistors showed high pH sensitivity as a result of the use of an interdigitated microchannel displaying high transconductance. Moreover, the modification of rGO FETs with a weak polyelectrolyte improved the pH response owing to its transducing properties by electrostatic gating effects. In the presence of urea, the transistors modified with $(polyethylenimine/urease)_n$ multilayer assemblies showed a shift in the Dirac point due to the change in the local pH close to the graphene surface, produced by the catalyzed urea hydrolysis. The transistors were able to monitor urea in the range of 1–1000 μm with a LOD of 1 μm, displaying a fast response and a good long-term stability. The enzyme surface coverage onto the channel was tuned by increasing the number of bilayers and thus incrementing the urea-response of the transistors. Heavy metal quantification in aqueous solution was performed taking advantage of the urease specific inhibition. We believe that the LbL assembly approach can expand the frontiers of graphene-based transistors by virtue of the wide variety of nanomaterials (nanoparticles, proteins, polymers, etc) suitable for being integrated using this technique.

Acknowledgements

This work was supported by the European Union's Horizon 2020 under the Marie Curie grant agreement No. 645686, CONICET, ANPCyT (PICT-2010-2554, PICT-2013-0905), the Austrian Institute of Technology GmbH (AIT–CONICET Partner Group, Exp. 4947/11, Res. No. 3911, 28-12-2011), Universidad Nacional de La Plata (UNLP), the Austrian Federal Ministry for Transportation, Innovation and Technology (GZ BMVIT-612.166/0001-III/I1/2010), by the FFG within the comet program, and from the governments of Lower and Upper Austria. E.P. acknowledges CONICET for a scholarship. C.B. acknowledges the financial support given by the NÖ Forschungs - und Bildungsges.m.b.H. F.B. and O.A. are staff researchers of CONICET. We thank Josef Breu for supplying graphene oxide flakes.

Appendix A. Supplementary material

Supplementary data associated with this article can be found in the online version at doi:10.1016/j.bios.2016.10.035.

References

Ahmad, R., Tripathy, N., Park, J.-H., Hahn, Y.-B., 2015. Chem. Commun. 51, 11968–11971.
Ariga, K., Hill, J.P., Ji, Q., 2007. Phys. Chem. Chem. Phys. 9, 2319–2340.
Cai, B., Wang, S., Huang, L., Ning, Y., Zhang, Z., Zhang, G., 2014. ACS Nano 8, 2632–2638.
Carvounis, C.P., Nisar, S., Guro-Razuman, S., 2002. Kidney Int. 62, 2223–2229.
Choi, W., Lee, J., 2012. Graphene synthesis and applications. In: Nanomaterials and Their Applications. CRC Press
Cortez, M.L., De Matteis, N., Ceolín, M., Knoll, W., Battaglini, F., Azzaroni, O., 2014. Phys. Chem. Chem. Phys. 16, 20844–20855.
Decher, G., Hong, J.D., 1991. Ber. Bunsenges. Phys. Chem. Ber. Bunsenges. Phys. Chem. 95, 1430–1434.
Decher, G., Schlenoff, J.B., 2012. Multilayer Thin Films: Sequential Assembly of Nanocomposite Materialssecond. ed. WILEY-VCH Verlag GmbH & Co, Weinheim.
Dong, X., Shi, Y., Huang, W., Chen, P., Li, L., 2010. Adv. Mater. 22, 1–5.
Forrest, S.R., Elmore, B.B., Palmer, J.D., 2005. Appl. Biochem. Biotechnol. 121, 85–91.
Gómez-Navarro, C., Weitz, R.T., Bittner, A.M., Scolari, M., Mews, A., Burghard, M., Kern, K., 2007. Nano Lett. 7, 3499–3503.
He, Q., Sudibya, H.G., Yin, Z., Wu, S., Li, H., Boey, F., Huang, W., Chen, P., Zhang, H., 2010. ACS Nano 4, 3201–3208.
Hess, L.H., Lyuleeva, A., Blaschke, B.M., Sachsenhauser, M., Seifert, M., Garrido, J.A., Deubel, F., 2014. ACS Appl. Mater. Interfaces 6, 9705–9710.
Iost, R.M., Crespilho, F.N., 2012. Biosens. Bioelectron. 31, 1–10.
Kazakova, L.I., Shabarchina, L.I., Sukhorukov, G.B., 2011. Phys. Chem. Chem. Phys. 13, 11110–11117.
Kim, D., Sohn, Y., Il, Jung, J., Yoon, O.J., Lee, N., Park, J., 2013. Biosens. Bioelectron. 41, 621–626.
Krajewska, B., 2008. J. Enzym. Inhib. Med. Chem. 23, 535–542.
Krajewska, B., 2009. J. Mol. Catal. B: Enzym. 59, 9–21.
Lakard, B., Magnin, D., Deschaume, O., Vanlancker, G., Glinel, K., Demoustier-Champagne, S., Nysten, B., Jonas, A.M., Bertrand, P., Yunus, S., 2011. Biosens. Bioelectron. 26, 4139–4145.
Marchenko, S.V., Kucherenko, I.S., Hereshko, A.N., Panasiuk, I.V., Soldatkin, O.O., El'skaya, A.V., Soldatkin, A.P., 2015. Sens. Actuators B Chem. 207, 981–986.
Melzer, K., Bhatt, V.D., Jaworska, E., Mittermeier, R., Maksymiuk, K., Michalska, A., Lugli, P., 2016. Biosens. Bioelectron. 84, 7–14.
Nguyen, N.S., Das, G., Yoon, H.H., 2016. Biosens. Bioelectron. 77, 372–377.
Niyogi, S., Bekyarova, E., Itkis, M.E., Zhang, H., Shepperd, K., Hicks, J., Sprinkle, M., Berger, C., Lau, C.N., Deheer, W.A., Conrad, E.H., Haddon, R.C., 2010. Nano Lett. (10), 4061–4066.
Ohno, Y., Maehashi, K., Yamashiro, Y., Matsumoto, K., 2009. Nano Lett. (9), 3318–3322.
Pallarola, D., Queralto, N., Battaglini, F., Azzaroni, O., 2010. Phys. Chem. Chem. Phys. 12, 8071–8083.
Pan, T.M., Lin, J.C., Wu, M.H., Lai, C.S., 2009. Biosens. Bioelectron. 24, 2864–2870.
Parviz, D., Das, S., Ahmed, H.S.T., Irin, F., Bhattacharia, S., Green, M.J., 2012. ACS Nano

6, 8857–8867.
Piccinini, E., Pallarola, D., Battaglini, F., Azzaroni, O., 2015. Chem. Commun. 51, 14754–14757.
Rajesh, B.V., Takashima, W., Kaneto, K., 2005. Biomaterials 26, 3683–3690.
Reiner-Rozman, C., Larisika, M., Nowak, C., Knoll, W., 2015. Biosens. Bioelectron. 70, 21–27.
Rydzek, G., Ji, Q., Li, M., Schaaf, P., Hill, J.P., Boulmedais, F., Ariga, K., 2014. Nano Today 10, 138–167.
Sant, W., Temple-Boyer, P., chanie, E., Launay, J., Martinez, A., 2011. Sens. Actuators B Chem. 160, 59–64.
Scouten, W.H., Luong, J.H.T., Stephen Brown, R., 1995. Trends Biotechnol. 13, 178–185.
Sheldon, R.A., Van Pelt, S., 2013. Chem. Soc. Rev. Chem. Soc. Rev. 42, 6223–6235.
Singh, M., Verma, N., Garg, A.K., Redhu, N., 2008. Sens. Actuators B Chem. 134, 345–351.
Sohn, I.Y., Kim, D.J., Jung, J.H., Yoon, O.J., Nguyen Thanh, T., Tran Quang, T., Lee, N.E., 2013. Biosens. Bioelectron. 45, 70–76.
Tsai, H.C., Doong, R.A., 2005. Biosens. Bioelectron. 20, 1796–1804.
Von Harpe, A., Petersen, H., Li, Y., Kissel, T., 2000. J. Control. Release 69, 309–322.
Wang, Y.Y., Burke, P.J., 2013. Appl. Phys. Lett., 103.
Wang, Y.Y., Burke, P.J., 2014. 7, 1650–1658.
Wong, H.-S., Akinwande, D., 2011. Carbon Nanotube and Graphene Device Physics. Cambridge University Press.
Yan, F., Zhang, M., Li, J., 2014. Adv. Healthc. Mater. 3, 313–331.
Yang, C.M., Wang, I.S., Lin, Y.T., Huang, C.H., Lu, T.F., Lue, C.E., Pijanowska, D.G., Hua, M.Y., Lai, C.S., 2013. Sens. Actuators B Chem. 187, 274–279.
Zhan, B., Li, C., Yang, J., Jenkins, G., Huang, W., Dong, X., 2014. Small 10, 4042–4065.
Zhang, M., Liao, C., Mak, C.H., You, P., Mak, C.L., Yan, F., 2015. Sci. Rep. 5, 8311.
Zhybak, M., Beni, V., Vagin, M.Y., Dempsey, E., Turner, A.P.F., Korpan, Y., 2016. Biosens. Bioelectron. 77, 505–511.